

# Neutrinos from the Propagation of a Relativistic Jet Through a Star

Jason Pruet

*N-Division, Lawrence Livermore National Laboratory, Livermore CA 94550*

## ABSTRACT

We discuss the neutrino signature of a relativistic jet propagating through a stellar envelope, a scenario realized in the collapsar model for Gamma Ray Bursts (GRBs). It is shown that the dramatic slowing of the jet deep within the star is accompanied by inelastic neutron-nucleon collisions and the conversion of a substantial fraction of the jet kinetic energy to neutrinos. These neutrinos have observed energies in the range two to tens of GeV and an estimated detection rate comparable to or larger than the detection rate of GeV neutrinos from other GRB-related processes. The time delay between the arrival of these neutrinos and the GRB photons is tens of seconds. An observation of this delay would provide an indication that the GRB jet originated in a massive star.

*Subject headings:* gamma rays: bursts—neutrinos

## 1. INTRODUCTION

In this paper we discuss neutrino production in collapsars (Woosley 1993; MacFadyen & Woosley 1999). Collapsars, or failed supernovae, are one of two or a few currently favored explanations for the origin of long duration GRBs. In collapsars, the relativistic jet which shocks and ultimately gives rise to observed GRB photons must first pass through a massive stellar mantle. Here it is shown that this passage is associated with an interesting neutrino signal.

A number of GRB-related neutrino sources have been previously investigated. These sources can be roughly divided according to whether they involve pion production via photomeson interactions or via strong interactions. Neutrinos resulting from photomeson interactions typically have very high energies ( $> 10^2$  TeV) and are possibly the most easily detectable in planned km-scale neutrino detectors such as ICECUBE (Halzen 1999). Waxman & Bahcall (1997) discussed photomeson production of neutrinos in collisionless GRB shocks and argued that detection of these neutrinos would give information on the spectra of

photons and protons within the shocks, as well as place stringent constraints on fundamental neutrino properties.

Neutrinos from inelastic nuclear collisions typically have energies of the order of 10 GeV. Unless the phototube density in ICECUBE and other next generation neutrino telescopes is higher than currently planned, these detectors will have a small effective detector area for such low energy neutrinos and will not be sensitive to them (Karle 2002). However, there is a growing indication that, like neutrinos from  $p - \gamma$  interactions, these neutrinos may be an important clue to conditions in and around the GRB central engine. Bahcall & Mészáros (2000) discussed the neutrino signal from inelastic collisions occurring during the dynamic decoupling of neutrons in the acceleration stage of the evolution of a GRB fireball. These neutrinos offer an indication of the composition and Lorentz factor of the GRB jet. Neutron diffusion in GRB environments was considered in a more general context by Mészáros & Rees (2000). Those authors showed that internal shocks at radii  $r \sim 3 \cdot 10^{11}$  cm and transverse diffusion of neutrons into the jet at much larger radii can lead to an appreciable neutrino signal. The possibility of using neutrinos to distinguish between collapsars and supernovae (Vietri & Stella 1998, 1999) was discussed by Guetta & Granot (2002). The scenario envisaged by Guetta and Granot is unique in that it predicts TeV neutrinos from nuclear processes. This is because of the presence in their model of protons accelerated to very high energies in a pulsar wind bubble.

The multi-GeV collapsar neutrino signal we study here is related to the mechanism giving rise to the variation in Lorentz factor of the outgoing jet. As with any GRB model invoking internal shocks, the jet variability must be substantial in order to explain observed temporal variability in GRBs, as well as to allow efficient conversion of kinetic energy to electromagnetic energy (see Piran (1999) for a general overview). In most GRB models, the jet variability is related to a variability in the mass ablation rate or luminosity of the central source driving the outflow. By contrast, the jet variability in the collapsar can arise from instabilities along the jet-stellar wall interface (Zhang, Woosley, & MacFadyen 2003). These instabilities operate at radii large compared to the size of the central black hole. Consequently, the instabilities act to slow a jet which has already had ample time to reach ultra-relativistic velocities. We point out that when free neutrons are present in the jet, this slowing is not elastic and is accompanied by a sizeable neutrino flux.

In the next section we discuss details of how the slowing of the neutrons in the jet leads to the conversion of jet energy to potentially observable neutrinos. Estimates of neutrino detection rates and energies are presented. We will show that the neutrino signal of the slowing of the jet can originate from radii some two orders of magnitude smaller than the signal of processes discussed by Mészáros & Rees (2000). Also, the neutrino production we

discuss here is relatively insensitive to the bulk Lorentz factor of the outgoing jet, unlike other proposed sources of multi-GeV GRB neutrinos.

## 2. Pion and Neutrino Production Deep Within the Collapsar

The mechanism giving rise to the variability in the outgoing jet can be crudely represented as the closing of a dense door composed of stellar material at some point along the jet axis. This results in a forward shock propagating into and accelerating the stellar material, and a reverse shock propagating backwards and slowing the jet. Because the stellar material blocking the passage of the jet is typically very dense relative to the jet material, the forward shock will only be mildly relativistic and uninteresting as far as a detectable neutrino signature is concerned. The top panel of Fig. 1 illustrates the shocking and structure of the outgoing jet.

As particles in the jet traverse the reverse shock, they are decelerated from a Lorentz factor  $\Gamma_j^{(L)}$  to a Lorentz factor  $\Gamma_{sh}^{(L)} < \Gamma_j^{(L)}$ . Here the superscript ( $L$ ) denotes a quantity as measured in the rest frame of the collapsing star. The relative Lorentz factor across the shock is  $\Gamma_{rel} \approx \Gamma_j^{(L)}/2\Gamma_{sh}^{(L)}$ . Numerical simulations of relativistic jets propagating in stars indicate that the typical relative Lorentz factor is substantial. Zhang et al. studied the propagation of a relativistic jet in a  $15M_\odot$  star for 3 different initial jet conditions. Typical values of  $\Gamma_{rel}$  for their simulations are given in Table 1. The simulations of Zhang et al., as well as observations of many peaks in observed GRB lightcurves, indicate that a substantial fraction (half or more) of the jet undergoes a slowing via relativistic shocks.

The gross properties of the reverse shock slowing the jet are given by the Rankine-Hugoniot jump conditions. In particular, the proper baryon number density in the shocked jet (i.e. the baryon number density as measured in a frame comoving with the shocked fluid) is  $n_{sh} \approx 4\Gamma_{rel}n_j$ , where  $n_j$  is the proper baryon number density in the unshocked jet. For radii larger than  $\approx 10^6\Gamma_j^{(L)}\text{cm}$ , which is the region of interest in the present work, the outgoing jet is coasting rather than accelerating (Piran, Shemi, & Narayan 1993). In the coasting regime,  $n_j$  is determined by baryon number conservation as  $n_j = L/4\pi r^2 m_N c^3 (\Gamma_j^{(L)})^2$ . Observations of GRBs suggest that the isotropic equivalent luminosity  $L$  is of order  $L \gtrsim 10^{52}\text{erg/sec}$  (Frail et al. 2001), and that typically  $\Gamma_j^{(L)} \gtrsim 200$  (Lithwick & Sari 2001). The energy density in the shocked jet fluid is  $U_{sh} \approx \Gamma_{rel}n_{sh}m_Nc^2$ , provided that the specific enthalpy in the unshocked jet is small (i.e. that the jet is in the coasting regime). In the middle panel of Fig. 1 we show the evolution of  $n_j$  and  $\Gamma_j^{(L)}$  in the jet.

Pion production and associated neutrino production in the reverse shock depend in detail

on the processes mediating the shock. It is convenient in discussing the shock structure to consider separately those particles which interact electromagnetically (protons- $e^\pm$ -photons) and the neutrons. Neutrons can only be slowed by strong collisions with other nucleons. Because the length scales associated with electromagnetic processes are small compared to the neutron mean free path, an upper limit to the width of the shock can be obtained by considering the case where strong nucleon-nucleon collisions alone mediate the shock. Such collisional shocks have been studied by Mott-Smith (1951) in the non-relativistic case and by Chapline & Weaver (1979) and Cercignani & Majorana (1988) in the relativistic case.

We take as an upper limit to the shock width the collisional width  $\delta_c \approx 1.9/\Gamma_{rel}n_j\sigma_{NN}$  found from the Monte-Carlo simulations of Chapline & Weaver (1979). Here  $\sigma_{NN}$  is the strong scattering cross section and the shock width is as measured in a frame comoving with the shock. For center of mass energies a few hundred MeV above the threshold for pion production,  $\sigma_{NN} \approx 4 \cdot 10^{-26}cm^2$ , and approximately 80% of this cross section goes towards inelastic production of pions (see Hagiwara et al. (2002) for a compilation of strong cross sections). For this work, the important properties of  $\delta_c$  are I) that because the shock width is at most a few collisional mean free paths, the neutron-nucleon collisions slowing the shock are hard and produce pions, and II) because  $\delta_c \propto 1/n_{sh}\sigma_{NN}$ , the number of inelastic collisions suffered by a typical neutron in traversing the shock is approximately independent of  $\Gamma_{rel}$ . A close-up view of inelastic neutron-nucleon collisions and associated pion production in the reverse shock is shown in the bottom panel of Fig. 1.

Protons in the shock will be slowed by electromagnetic, rather than strong, processes. Deep within the star, where the shocks considered in this paper are occurring, the plasma is optically thick and the thermalization time for radiation is short. Consequently, we approximate the protons as being in thermal equilibrium with the background  $e^\pm/\gamma$  plasma<sup>1</sup>. The temperature of the protons in this case is small,  $kT \ll m_p c^2$ , and the protons are non-relativistic in the shocked plasma frame.

Our assumption about the proton distribution function is in accord with results from studies of shock propagation in type II SNe (e.g. Ensman & Burrows (1992)). However, Mészáros & Waxman (2001) have argued that protons shocked in mildly relativistic collisions at large radii inside the collapsar will be driven to a power law distribution, but that protons shocked in the strongly relativistic collision between the jet head and the stellar mantle may or may not have a power law distribution. The question of the precise radius (presumably

---

<sup>1</sup>The opposite limiting case for the proton distribution is that where the protons are Fermi-accelerated and achieve a power law distribution. In this case, the maximum proton energy (typically much larger than the proton rest mass) is that for which the acceleration and cooling times are equal (Waxman 1995).

larger than  $10^{11}\text{cm}$ ) at which shocks are collisionless rather than radiative is not addressed here. As we are most interested in processes at  $r \lesssim 10^{11}\text{cm}$ , this issue is not so important for the present study.

In the inelastic collisions slowing the neutrons, the total energy going into pion production in the center of mass frame of the collision is  $E_\pi^{tot} \approx (1/2)(E_{cm} - 2m_N c^2)$  (e.g. Mannheim & Schlickeiser (1994)). Here  $E_{cm}$  is the energy of the collision in the center of mass frame, and the above equation is valid provided that  $E_{cm} - 2m_N c^2$  is larger than a few times the pion rest mass energy. Very near the threshold for pion production,  $E_\pi^{tot} \approx E_{cm} - 2m_N c^2$ . The average energy of individual pions created in the collision is  $E_\pi^{tot}/\xi$ , where  $\xi$  is the multiplicity of produced pions. As measured in a frame at rest with respect to the star, the energy of pions produced in a neutron-nucleon collision is

$$E_\pi^{(L)} = \Gamma_{cm} E_\pi^{(tot)} = \left( \frac{m_N c^2}{2} \right) \left( \Gamma_j^{(L)} + \Gamma_{sh}^{(L)} - 2\Gamma_{cm} \right). \quad (1)$$

Here we have made the assumption that the typical collision occurs between a nucleon with Lorentz factor  $\Gamma_j^{(L)}$  and a nucleon with Lorentz factor  $\Gamma_{sh}^{(L)}$ . In Eq. 1,  $\Gamma_{cm}$  is the Lorentz factor of the center of mass frame as measured in the lab frame. In terms of the Lorentz factors of the unshocked and shocked portions of the jet,  $\Gamma_{cm} \approx \sqrt{\Gamma_j^{(L)} \Gamma_{sh}^{(L)}}$  if  $\Gamma_{sh}$  is larger than two or three, and  $\Gamma_{cm} \approx \sqrt{\Gamma_j^{(L)}/2}$  if  $\Gamma_{sh} \approx 1$ . The observed energy of an individual pion created in a collision will again be a factor of  $1/\xi$  smaller than the estimate in Eq. 1. For example, for  $\Gamma_j^{(L)} = 100$ ,  $E_\pi^{(L)}/\xi \approx 10, 12,$  and  $7$  GeV, for  $\Gamma_{sh} = 30, 10,$  and  $1$  respectively.

The neutrino signal of the inelastic collisions depends on how the spectrum of pions produced in these collisions is modified by cooling processes. Pion cooling may proceed through inelastic strong scatterings, or via electromagnetic interactions - coulomb scattering off the background electrons, inverse compton scattering, and synchrotron emission.

Cooling via strong scatterings is simply characterized by the  $\pi$ -nucleon interaction time. We can roughly approximate  $\pi - N$  collisions as occurring in the shocked region (as opposed to the region of width  $\delta_c$  characterizing the shock). In this case the  $\pi$ -nucleon interaction time is

$$\tau_{\pi-N} = \frac{1}{c\sigma_{N\pi}n_{sh}}, \quad (2)$$

where  $\sigma_{N\pi}$  is the nucleon-pion scattering cross section. For center of mass energies a few hundred MeV larger than the pion rest mass,  $\sigma_{N\pi} \approx 2.5 \cdot 10^{-26}\text{cm}^2$  (Hagiwara et al. 2002). As with NN collisions, the bulk of this cross section goes toward inelastic  $\pi$  production. Though inelastic  $\pi N$  collisions may roughly conserve the total energy in pions, they tend to reduce the average pion energy, making detection of the product neutrinos more difficult. Note that because  $\sigma_{N\pi}$  and  $\sigma_{NN}$  are comparable, a more accurate expression for  $\tau_{\pi-N}$  should

involve an effective nucleon number density within the region of width  $\delta_c$  (rather than the  $n_{sh}$  appearing in Eq. 2). Because the number density within the shock is smaller than  $n_{sh}$ , Eq. 2 represents a lower bound on  $\tau_{\pi-N}$  (or an upper limit on the influence of  $\pi N$  scatterings).

Pion energy loss via coulomb scattering off the background electrons is given by the Bethe-Bloch formula for ionization losses (see Groom et al. (2000)), with the ionization potential for completely ionized material equal to  $\hbar\omega_p$ . Here  $\omega_p = \sqrt{4\pi n_e e^2/m_e}$  is the electron plasma frequency, and  $n_e$  is the electron number density. Neglecting an unimportant (for our applications) logarithmic dependence on  $n_e$ , pion energy loss via coulomb scattering is given by  $dE/dx \approx (2/3) \cdot 10^{-26} n_e \text{ GeV/cm}$ . The timescale for energy loss via  $\pi - e^-$  scatterings is then  $\tau_{\pi-e^-} \approx (\Gamma_\pi/2)(n_{sh}/n_e)\tau_{\pi-N}$ , with  $\Gamma_\pi$  the pion Lorentz factor as measured in the shocked fluid frame. When strong scatterings are inefficient at cooling the pions, the temperature in the shocked plasma is generally too low for efficient pair  $e^\pm$  production. In this case  $n_e \lesssim n_{sh}$  and  $\pi - e^-$  interactions are at most only as important as strong scatterings. Pion energy loss via bremsstrahlung and pair production is not important for pion energies less than about 100 GeV (Groom et al. 2000).

Pions lose energy to the background photon and magnetic fields at a rate  $(dE_\pi/dt)_{\pi-\gamma} \approx (c\Gamma_\pi^2)(m_e/m_\pi)^2\sigma_T U_{em}$ , where  $\sigma_T$  is the Thomson cross section,  $m_\pi$  is the pion mass, and  $U_{em}$  is the energy density in the photon and magnetic fields. A cooling time  $\tau_{\pi-\gamma}$  can be defined as  $\tau_{\pi-\gamma} = E_\pi(dE_\pi/dt)_{\pi-\gamma}^{-1}$ . Cooling of pions via these electromagnetic interactions dominates over cooling via strong interactions when

$$\left(\frac{\Gamma_\pi}{400}\right)\left(\frac{U_{em}}{n_{sh}m_Nc^2}\right) \approx \left(\frac{\Gamma_{rel}\Gamma_\pi}{400}\right) < 1. \quad (3)$$

Here we have made use of the fact that  $U_{em} \sim U_{sh}$  for relativistic shocks in an optically thick flow. Only in some of the more extreme cases that we consider here is the above inequality not satisfied. By contrast, for shocks at large radii ( $r \sim 10^{12} \text{ cm}$ ) when the protons are accelerated to high energies via plasma processes, typical pions produced in photomeson interactions have Lorentz factors of  $\sim 10^6$ , and synchrotron cooling is more important than strong scattering.

In the shocked plasma rest frame the lifetime of a charged pion is  $\tau_{\pi-D} = 2.6 \cdot 10^{-8} \Gamma_\pi \text{ s}$ . The fraction of pions that decay before suffering a strong scattering is  $1/(\tau_{\pi-D}/\tau_{\pi-N} + 1)$ . The pion Lorentz factor relative to the shocked plasma for which  $\tau_{\pi-D} = \tau_{\pi-N}$  is

$$\Gamma_{\pi,cool} \equiv 7 \cdot 10^2 \frac{(r/10^{10} \text{ cm})^2 (\Gamma_j^{(L)}/100)^2}{\Gamma_{rel} L_{52}}. \quad (4)$$

Pions with a Lorentz factor greater than  $\Gamma_{\pi,cool}$  will on average scatter before decaying, and pions with a Lorentz factor smaller than  $\Gamma_{\pi,cool}$  will on average decay before scattering. Eq.

4 indicates that for  $r \gtrsim 10^9$ cm, pions produced in mildly relativistic collisions ( $\Gamma_{rel} \sim 2$ ) will decay before cooling. Conversely, for  $r \sim 10^9$ cm, pions produced in strongly relativistic shocks ( $\Gamma_{rel} \gtrsim 10$ , as in case JA in the calculations of Zhang et al.) will cool before decaying. Neutrinos from the decay of cooled pions will typically have observed energies  $\lesssim 1$ GeV, and will be difficult to detect. For  $r \gtrsim 10^{10}$ cm, Eq. 4 indicates that pions produced even in very relativistic shocks will decay before cooling.

In Fig. 2 we show the ratios of the timescales for the pion cooling processes discussed above to the timescale for pion decay. For this figure we have approximated the electron and nucleon number densities in the post-shock region as being equal and we have also made the assumption that  $\Gamma_{rel} = \Gamma_{\pi}$ . As can be seen from Fig. 2, for  $\Gamma_{rel} = 2$  and  $r \gtrsim 1.5 \cdot 10^9 \sqrt{L_{52}}(100/\Gamma_j^{(L)})$ cm, pion cooling processes are unimportant (e.g. the timescale for all cooling processes is more than twice the decay timescale and less than 30% of the pion energy is lost). For  $\Gamma_{rel} = 10$ , pion cooling processes are unimportant for  $r \gtrsim 7 \cdot 10^9 \sqrt{L_{52}}(100/\Gamma_j^{(L)})$ cm.

On average, neutrinos carry away  $\sim 2/3$  of the pion energy. The typical energies of the three neutrinos the pion (and daughter muon) decays to are in the range 30-50MeV as measured in the pion rest frame. This implies observed neutrino energies in the range  $\sim [1/5 - 1/3](E_{\pi}^{(L)}/\xi)(1+z)^{-1}$ GeV, with  $z$  the redshift at which the burst occurs. In Table 1, typical neutrino energies for the different simulations of Zhang et al. are shown. Note that the observed neutrino energy scales linearly with jet Lorentz factor. For example, for  $\Gamma_j^{(L)} = 400$ , the expected neutrino energies are a factor of approximately four higher than shown in Table 1.

The fraction of jet kinetic energy lost to neutrinos is approximately

$$(1 - Y_e) \left(\frac{2}{3}\right) \left(\frac{2}{3}\right) \frac{E_{\pi}^{(L)}}{\Gamma_j^{(L)} m_N c^2} \quad (5)$$

for collisions occurring at radii large enough that the charged pions do not cool before decaying. Here the electron fraction  $Y_e$  is the ratio of protons to baryons in the flow. Recent studies indicate that the outgoing jet is likely neutron rich, with plausible values of  $Y_e$  in the range  $1/20 \lesssim Y_e \lesssim 1/2$  (Pruet, Woosley, & Hoffman 2002; Beloborodov 2002). In Eq. 5, one factor of  $2/3$  approximately accounts for the fraction of charged pions (as opposed to  $\pi^0$ 's) produced, while the other factor of  $2/3$  accounts for the fraction of the charged pion energy going to neutrinos. The estimate in Eq. 5 assumes that after one inelastic collision the decelerating neutron does not undergo subsequent inelastic collisions. For this reason, Eq. 5 represents a lower bound to the fraction of jet energy lost to neutrinos. The true fraction could be as much as a factor of  $\sim 2$  higher, depending on the jet composition and

details of the shocking. For the jet dynamics calculated by Zhang et al., estimates of the fraction of jet energy going to neutrinos lie in the range  $[0.1 - 0.2](1 - Y_e)$ .

To facilitate comparison with studies of other GRB related neutrino production processes, we closely follow the analysis and notation of Bahcall & Mészáros (2000) and Mészáros & Rees (2000) in estimating the neutrino detection rate. In the notation of those authors, the average neutrino detection rate of events at redshift  $z$  is  $R_\nu \approx (N_t/4\pi D^2)R_b N_n \sigma_{\nu\bar{\nu}}$ . Here  $N_t$  is the number of protons in the terrestrial detector,  $D$  is the proper distance out to redshift  $z$ ,  $R_b$  is the GRB rate within a Hubble radius, and  $N_n$  is the isotropic equivalent number of neutrons undergoing inelastic scattering. The neutrino detection cross section averaged over neutrinos and anti-neutrinos is  $\sigma_{\nu\bar{\nu}} \approx 0.5 \cdot 10^{-38} (\sum E_\nu/1\text{GeV})(1+z)^{-1}\text{cm}^2$  (Gaisser 1990), where  $\sum E_\nu \approx (2/3)E_\pi^{(L)}$  is the total energy of all neutrinos resulting from an inelastic neutron-nucleon collision. Using Eq. 1 and adopting an Einstein-de Sitter cosmology with Hubble constant  $H = 65h_{65}\text{km/s/Mpc}$  gives

$$R_\nu \approx 2E_{53}(1 - Y_e) \left( \frac{100}{\Gamma_j^{(L)}} \right) f_{shock} \left( \frac{E_\pi^{(L)}}{m_N c^2} \right) \left( \frac{N_t}{10^{39}} \right) \left( \frac{R_b}{10^3} \right) h_{65}^2 \left( \frac{2 - \sqrt{2}}{1 + z - \sqrt{1 + z}} \right)^2 \text{year}^{-1}. \quad (6)$$

Here  $E_{53}$  is the isotropic equivalent jet energy in units of  $10^{53}\text{erg}$ , and  $f_{shock}$  is the fraction of the jet undergoing a relativistic slowing at radii large enough the produced pions do not cool and decay to unobservable neutrinos ( $r \gtrsim 10^9\text{cm}$  for mildly relativistic collisions and  $r \gtrsim 10^{10}\text{cm}$  for ultra-relativistic collisions). For illustration, the models of Zhang et al. predict neutrino detection rates of  $\sim 21/\text{year}$  (JA),  $\sim 7/\text{year}$  (JB), and  $\sim 10/\text{year}$  (JC), for  $E_{53} = 1$ ,  $Y_e = 1/2$ , and  $f_{shock}=1/2$ . For model JB, where the relative Lorentz factors across the shock deep within the star are very similar to the relative Lorentz factors typical of internal shocks occurring at  $\sim 10^{11}\text{cm}$ , the expected detection rate is roughly the same as that calculated by Mészáros & Rees (2000) for neutrinos from internal shocks. For models JA and JC, in which the jet is more dramatically slowed, the expected detection rates are somewhat larger, approaching the sorts of detection rates expected for efficient sideways diffusion of neutrons into the jet.

As can be seen from Eq. 6,  $R_\nu$  does not depend explicitly on the beaming angle of emitted neutrinos. However, as we discuss below, a temporal and directional correlation between detected neutrinos and the parent GRB is needed in order to distinguish GRB neutrinos from background atmospheric neutrinos. If the beaming angle of emitted neutrinos ( $\Omega_\nu$ ) is smaller than the beaming angle of GRB photons ( $\Omega_\gamma$ ), then a parent GRB is always visible in coincidence with detected GRB neutrinos. If the opposite case holds ( $\Omega_\nu > \Omega_\gamma$ ), then those neutrinos emitted outside of the photon beaming angle are effectively lost to observation and the detection rate is effectively decreased by a factor of  $\Omega_\gamma/\Omega_\nu$ . Two competing



processes affect  $\Omega_\nu/\Omega_\gamma$ : the focusing of an initially wide jet as the jet propagates through the star (Aloy et al. 2000; Zhang, Woosley, & MacFadyen 2003), and the expansion of the high enthalpy jet as it breaks free of the star (Zhang, Woosley, & MacFadyen 2003). Jet focusing tends to increase  $\Omega_\nu/\Omega_\gamma$  because it makes the jet opening angle within the star larger than the jet opening angle at the stellar surface. Expansion of the high enthalpy jet tends to decrease  $\Omega_\nu/\Omega_\gamma$ . Present 2-d simulations of jet propagation do not definitively determine which process is dominant, though they are roughly consistent with  $(\Omega_\nu/\Omega_\gamma) \approx 1$ .

It should be emphasized that Eq. 6 and the detection rates estimated for GeV neutrinos from GRBs neglect many of the experimental difficulties associated with detecting these neutrinos. As noted in the introduction, the detector phototube spacing must be small enough to allow detection of  $\sim 10\text{GeV}$  muons with  $\sim 50\text{m}$  pathlengths (e.g. see Halzen & Hooper (2002)). In addition, the angle of the incident neutrino relative to the GRB must be sufficiently well known to distinguish a GRB neutrino from the background atmospheric neutrinos. Rough estimates can be made by scaling detection rates for Super-Kamiokande to the larger detectors discussed here. In the search through the Super-Kamiokande data for GRB neutrinos, a high-energy neutrino ( $E_\nu > 200\text{MeV}$ ) background rate of  $2 \cdot 10^{-3}(20 \text{ sec})^{-1}$  was assumed (Fukuda et al. 2002). Estimating that roughly 1/5 of these have energies larger than a few GeV, approximating the volume of a  $\text{km}^3$  detector as being  $\sim 10^5/5$  times larger than the volume of Super-Kamiokande, and supposing the angle of the incident neutrino relative to the GRB position is known to within a cone of  $\sim 10^\circ$  half-opening angle gives a background in a  $\text{km}^3$  detector of  $\approx 0.1(20 \text{ sec})^{-1}$ . With this background rate, a total sample of 1000 GRBs, and no other information, a detection of 20 neutrinos from 20 separate GRBs (out of a thousand) is not statistically significant, but the detection of two or three neutrinos from a single GRB is quite significant (see Table 1 in Fukuda et al. for detailed estimates). As a definite example of the potential of large neutrino detectors, the slowing of a relativistic jet in GRB 980425 ( $z = 0.0085$  (Galama et al. 1998)) should have given roughly 100 neutrino detections in a  $\text{km}^3$  detector. Even without directional information, such a detection would be significant.

### 3. Summary

Numerical simulations of the propagation of a relativistic jet through a stellar envelope indicate that, deep within the star, instabilities along the jet-stellar wall interface slow the jet. This slowing gives rise to a variation in the Lorentz factor of an initially uniform jet. As we have shown, the slowing of neutrons within the jet also gives rise to an interesting and potentially detectable neutrino signal.

Neutrinos produced during the slowing of the jet can precede GRB photons by tens to several tens of seconds, depending on the jet dynamics and stellar progenitor. By contrast, neutrinos produced in a jet that is not subsequently dramatically slowed arrive within  $\sim 0.3(r_\gamma/10^{12}\text{cm})(100/\Gamma_j^{(L)})$  seconds of the GRB photons, where  $r_\gamma$  is the radius where the jet shocks and produces observed photons. The observation of GeV neutrinos preceding a GRB flash by  $\sim 20$  seconds would be an indication that a relativistic jet had been slowed while optically thick. In turn, this could imply that the jet had punched through a stellar envelope.

Slowing of the jet within the star also has an impact on the jet composition. This is because neutron-neutron collisions, which dominate the slowing of neutrons if the jet is neutron rich, preferentially produce protons. Near threshold, for example, roughly 75% of the inelastic nn(pp) cross section goes toward the production of a p(n) (McGill et al. 1984). A jet born near the central black hole with a very low electron fraction will arrive at large radii with  $Y_e \sim 1/2$ . This will influence subsequent nucleosynthesis in the jet (Pruet, Guiles, & Fuller 2002; Lemoine 2002), as well as the production of neutrinos by inelastic nuclear processes at large radii.

Apart from composition effects, though, the source of GeV neutrinos we have discussed arises independently of other proposed sources of GeV neutrinos in relativistic fireballs. For example, neutron diffusion in internal shocks at  $r > 10^{11}\text{cm}$  or the transverse diffusion of neutrons into the jet at larger radii (Mészáros & Rees 2000), and inelastic nuclear collisions during neutron decoupling (Bahcall & Mészáros 2000), can still occur and produce neutrinos. In the most optimistic case where all of these various processes occur, the detection rate of neutrinos in a km-scale detector could be as high as 30 per year.

The author acknowledges helpful correspondence with Weiqun Zhang regarding the conditions in collapsar jets and several useful suggestions from the referee John Beacom. This research has been supported by the DOE Program for Scientific Discovery through Advanced Computing (SciDAC; DE-FC02-01ER41176). This work was performed under the auspices of the U.S. Department of Energy by University of California Lawrence Livermore Laboratory under contract W-7405-ENG-48.

## REFERENCES

- Aloy, M. A., Müller, E., Ibáñez, J. M., Martí, J. M., & MacFadyen, A. I. 2000, *ApJ*, 531, L119.
- Bahcall, J. N. & Mészáros, P. 2000, *Phys. Rev. Lett.*, 85, 1362

- Beloborodov, A. M. 2002, astro-ph/0209228
- Cercignani, C. & Majorana, A. 1988, *Physics of Fluids*, 31, 1064
- Chapline, G.F. & Weaver, T.A. 1979, *Physics of Fluids*, 22, 1884
- Ensmann, L. & Burrows, A. 1992, *ApJ*, 392, 742
- Frail, D.A. et al. 2001, *ApJ*, 562, L55
- Fukuda, S. et al. (the Super-Kamiokande collaboration) 2002, *ApJ*, 578, 317
- Galama et al. 1998, *Nature*, 395, 670
- Hagiwara et al. (Particle Data Group) 2002, *Phys. Rev. D*, 66, 010001.
- Gaisser, T. K. 1990, *Cosmic Rays and Particle Physics* (Cambridge: Cambridge Univ. Press)
- Groom, D.E. et al. 2000, *European Physical Journal*, C15, 1
- Guetta, D. & Granot, J. 2002, astro-ph/0212045
- Halzen, F. 1999, astro-ph/9908138
- Halzen, F. & Hooper, D. 2002, *Rept. Progr. Phys.* 65, 1025
- Karle, A. for the ICECUBE collaboration 2002, astro-ph/0209556
- Lithwick, Y. & Sari, R. 2001, *ApJ*, 555, 540
- Lemoine, M. 2002, *A&A*, 390, L31
- MacFadyen, A. I., & Woosley, S. E. 1999, *ApJ*, 524, 262
- McGill, J. A. et al. 1984, *Phys. Rev. C*, 29, 204
- Mannheim, K. & Schlickeiser, R. 1994, *A&A*, 286, 983
- Mészáros, P. & Rees, M.J. 2000, *ApJ*, 541, L5
- Mészáros, P. & Waxman, E. 2001, *Phys. Rev. Lett.*, 87, 1102
- Mott-Smith, H.M. 1951, *Physical Review*, 82, 885
- Piran, T., Shemi, A., & Narayan, R. 1993, *MNRAS*, 263, 861
- Piran, T. 1999, *Phys. Rep.*, 314, 575

- Pruet, J., Guiles, S., & Fuller, G. M. 2002, ApJ, 580, 368
- Pruet, J., Woosley, S.E., & Hoffman, R.D. 2002, ApJ, in press
- Vietri, M., & Stella, L. 1998, ApJ, 507, L45
- Vietri, M., & Stella, L. 1999, ApJ, 527, L43
- Waxman, E. 1995, Phys. Rev. Lett., 75, 386
- Waxman, E. & Bahcall, J. 1997, Phys. Rev. Lett., 78, 2292
- Woosley, S. E. 1993, ApJ, 405, 273
- Zhang, W., Woosley, S. E., & MacFadyen, A.I. 2003, ApJ, 586, 356

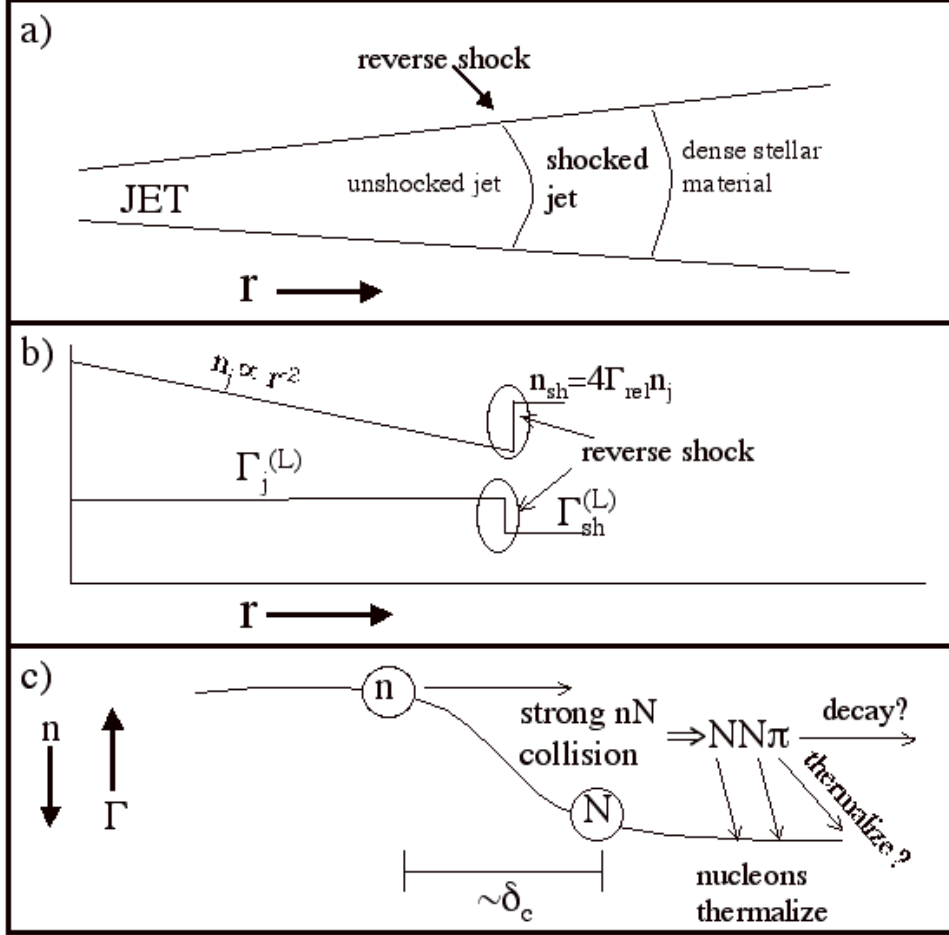


Fig. 1.— Illustration of the jet shocking and shock structure. Panel a) shows the shocking of the jet propagating through the stellar envelope. In this paper we are concerned with shocks occurring between  $r \sim 10^9 - 10^{11}$  cm. Panel b) shows the the baryon number density ( $n$ ) and jet Lorentz factor ( $\Gamma$ ) in the un-shocked (subscript  $j$ ) and shocked (subscript  $sh$ ) regions. Panel c) shows a close-up of the reverse shock (circled region in panel b). In panel c) the shock width is  $\delta_c$ . This is the typical length over which the neutron-nucleon collisions slowing the jet occur. Neutrons will eventually thermalize with the plasma in the shocked jet region. Depending on the details of the shocking, pions created in inelastic neutron-nucleon collisions may or may not thermalize before decaying.

Table 1. Estimates of properties of the neutrino signal from jets with different initial conditions propagating through a star.

Model <sup>a</sup>	$\Gamma_{rel}$ <sup>b</sup>	$E_\nu(1+z)$ <sup>c</sup>	$R_\nu$ <sup>d</sup>
JA	$\sim 6 - 50$	2-3	21
JB	$\sim 2 - 3$	5-8	7
JC	$\sim 4 - 9$	2-3	10

<sup>a</sup>Models refer to the different models calculated in Zhang, Woosley, & MacFadyen (2003)

<sup>b</sup>Typical Lorentz factors across the shocks slowing the jet within the star from the simulations of Zhang et al.

<sup>c</sup>Our calculation of the typical range of energy in GeV of neutrinos created in the shock slowing the jet as seen by an observer at rest with respect to the star.

<sup>d</sup>Our estimate of the annual detection rate of neutrinos with energies of a few GeV in a km-scale detector. In this estimate,  $z = 1$ ,  $Y_e = 1/2$ ,  $E = 10^{53}$ erg, and  $f_{shock} = 1/2$  are assumed.

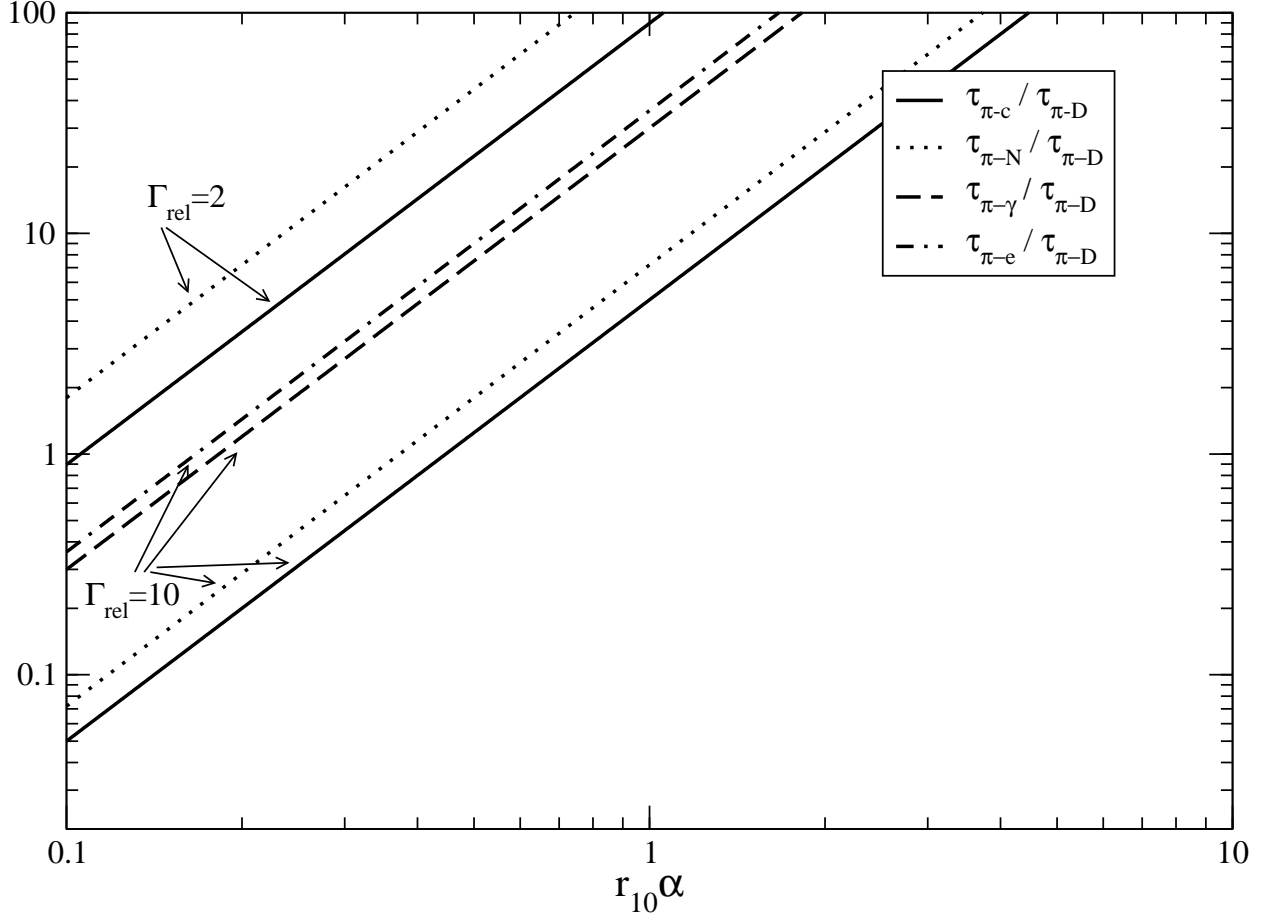


Fig. 2.— Illustration of the ratio of the timescales governing the various cooling processes to the timescale for pion decay. Here  $\alpha = (1/\sqrt{L_{52}})(\Gamma_j^{(L)}/100)$ . The total cooling timescale is  $\tau_{\pi-c} = (\tau_{\pi-N}^{-1} + \tau_{\pi-\gamma}^{-1} + \tau_{\pi-e}^{-1})^{-1}$ . For the  $\Gamma_{rel} = 2$  curves,  $\tau_{\pi-\gamma}/\tau_{\pi-D}$  is too large to appear on this graph, and the  $\tau_{\pi-N}/\tau_{\pi-D}$  curve exactly overlaps with the  $\tau_{\pi-e}/\tau_{\pi-D}$  curve.